Direct Observation of Three Chiral Conformers of an Atomically Precise Metal Nanoparticle

Anish Kumar Das,[a,c†] Swastik Hegde,[b,c†] Toby J. Woods,[a] Vaibhav S. Wani,[d] Mikael P. Backlund[a,b,c*]

[a] Department of Chemistry, University of Illinois at Urbana-Champaign, Urbana, Illinois 61801, USA

[b] Center for Biophysics and Quantitative Biology, University of Illinois at Urbana-Champaign, Urbana, Illinois 61801, USA

[c] Illinois Quantum Information Science and Technology Center, University of Illinois at Urbana-Champaign, Urbana, Illinois 61801, USA

[d] Department of Chemistry, Brown University, Providence, Rhode Island 02912, USA

† The authors contributed equally.

*mikaelb@illinois.edu

Abstract

Atomically precise nanoclusters (NCs) have attracted a lot of attention owing to their many interesting properties and applications. Although such clusters could be considered small molecules due to their discrete atomic compositions, their size and complexity push them into a distinct regime where the line between molecule and material is blurred. On the fundamental side, they can provide a testbed for understanding structure-property relationships in nanomaterials. Hence, their isomerism is of intrinsic significance. In this work, we report the atomically precise structure of three Cu_{14} NC conformers, *i.e.,* NCs with the same chemical formula and atomic connectivity but with varying bond angles and distances, obtained through X-ray crystallography. Interestingly, all three conformers exhibit chirality and co-crystallize in the same lattice structure. Since interconversion of each conformer and its chiral counterpart is possible without breaking and remaking bonds, these NCs constitute a set of atropisomers. The structure of our Cu_{14} NC highlights the various sources of isomerism one can observe at the nanoscale. These subtle yet identifiable differences represent something like a minimal unit of structural change, facilitating future investigation of structure-property relationships.

Keywords: Nanocluster, atom-precise, conformer, chirality, atropisomerism, co-crystallization

Conformational isomerism, a fundamental concept in structural chemistry, is best understood in the context of small (*i.e.,* containing less than a few dozen atoms) molecules having readily accessible crystallographic structures.[1] Extending this concept to the nanoscale—here defined as molecules or clusters with dimensions typically between 1 and 100 nm-- is nontrivial due to the inherent difficulty in obtaining precise atomic structures of these species.[2] Recent advances in atomically precise metal nanoclusters (NCs) have opened doors in this regard.[3-8] These nm-sized molecules, consisting of a few to hundreds of metal atoms protected by organic ligands, are amenable to X-ray crystallographic studies, and therefore their structures can be determined with atomic precision.[9-11] A growing database of atomically precise metal NCs so far includes at least a dozen structural isomers (and a similar number of stereoisomers).[12-20] Most of these documented structural isomers have different atom connectivity and thus do not qualify as conformational isomers (or conformers).

Conformational isomerism arises from free rotation about single bonds, which allows molecules to adopt different spatial arrangements.[21-24] For example, in small molecules like butane, rotation around the C-C single bond gives rise to anti, gauche, and eclipsed conformations. Unlike transient structural arrangements resulting from thermal vibrations and rotations, conformers correspond to stable atomic arrangements located at some energy minima. In the case of larger, more complex structures such as nanometer-sized macromolecules, the same core idea should translate—conformers must share the same atom connectivity but differ in spatial arrangements. Structural rearrangements of enzymes and other biological macromolecules can be regarded as a form of conformational isomerism in this vein.[25] Understandably, conformational changes of nanoscale macromolecules are more likely to involve variation in many bond lengths and angles, as opposed to the simple rotations observed in smaller molecules.

Although there is no dearth of examples of structural isomerism in NCs, to the best of our knowledge there exist two reports of conformers to date, both of which involve a change in only ligand arrangement.[26,27] In this work, we report three conformers of Cu_{14} NC with meticulous bond length and angle tabulation. The conformers differ in core Cu-Cu distances, Cu-S bonds, and ligand arrangement while maintaining the same atom connectivity. A recent related work reported a similar Cu_{14} skeleton with different ligands, but which did not exhibit this type of conformational isomerism.[28]

While the existence of NC conformers in the liquid or gas state may be expected, direct observation of their co-crystallization is surprising, as the process of crystallization tends to pick one conformer over all others. We hypothesize that this observation is facilitated by a reduction in total crystalline energy due to favorable packing and despite discrepancies in the energies of the individual conformers. Our observation is distinct from that reported in a previous study in which two conformers of the same molecule were obtained in separate crystals.[26]

Each of the three conformers we observe are chiral. Since it is possible to interconvert between two chiral conformers without breaking and re-making bonds, they can technically be classified as atropisomers.[22] Atropisomerism is a subset of chirality arising from restricted rotation rather than the presence of stereocenters. To the best of our knowledge this is the first case of atropisomerism in nanoclusters, effectively bridging a molecular-level phenomenon to the nanoscale.

By demonstrating how bond length variations, angular distortions, and ligand arrangements coalesce into distinct conformers, this study pushes the boundaries of what is achievable in structural chemistry. It serves as a useful guide to the taxonomy of isomerism as it applies to the nanoscale. Looking forward, it provides a concrete system in which the physical and chemical consequences of subtle structural differences—otherwise challenging to observe in nanoscale systems—can be directly studied with atomic precision.

Results and discussion

Copper NC was synthesized by dissolving $Cu(CH_3CN)_4.BF_4$, triphenylphosphine (PPh_3), and isopropyl thiol (^{i}PrSH) in a mixture of acetonitrile (CH_3CN) and chloroform ($CHCl_3$). Methanolic $NaBH_4$ was then added under vigorous stirring at room temperature, triggering the reaction that yielded an orange precipitate after an hour. This precipitate was collected, dried, and subsequently dissolved in a $CHCl_3$/hexane mixture. By allowing the solution to evaporate slowly over five days, we obtained high-quality yellow prism-shaped crystals of micrometer size.

Single-crystal X-ray diffraction (SC-XRD) analysis, mass spectrometry, and NMR collectively confirmed the molecular formula of the synthesized Cu NC to be $[Cu_{14}(^i PrS)_3(PPh_3)_8H_{10}]\cdot BF_4\cdot(CHCl_3)$ (henceforth referred to as **Cu_{14}**). Positive-mode electrospray ionization mass spectrometry (ESI-MS) displayed two prominent peaks. The peak at mass-charge ratio m/z 3223.40 is consistent with the main molecular formula $[Cu_{14}(^i PrS)_3(PPh_3)_8H_{10}]^+$ (Figure 1a). The second peak at m/z 2960.80 corresponds to $[Cu_{14}(^i PrS)_3(PPh_3)_8H_{10} - (PPh_3)]^+$, fragment of the main cluster (Figure S1). The experimental isotopic pattern matched the simulated spectra for both peaks (Figures 1 inset & S1).

The presence of 10 hydrides was confirmed using mass spectrometry and NMR. We synthesized the deuteride analogue of the Cu_{14} NC by employing $NaBD_4$ as the reducing agent instead of $NaBH_4$. The ESI-MS of the deuteride analogue exhibited a peak at m/z 3233.26 corresponding to the $[Cu_{14}(^i PrS)_3(PPh_3)_8D_{10}]^+$ along with its fragment peak. The corresponding peak shift of $\Delta m/z \approx 9.86$ indicates the replacement of 10

hydrides with 10 deuterides (Figure S2). This was further supported by the ^{2}H-NMR spectrum, which displayed four distinct peaks with intensity ratios of 1:3:3:3 (Figure S3).

SC-XRD analysis revealed that the Cu_{14} NC crystallizes in the trigonal crystal system with a chiral space group $P3_1c$ (Table S1). SC-XRD data (R_1 = 2.85%) revealed the presence of three distinct structures, which we denote as clusters A, B, and C. We use "cluster A, B, C" and "conformer A, B, C" interchangeably throughout the manuscript. The asymmetric unit consists of fragments of all three clusters (Figure S4). The three clusters share a similar structural framework with the same atom connectivity but different interatomic lengths and angles, *i.e.,* they are conformers of one another.

For illustrative purposes, we focus on cluster C to highlight the common underlying structure (Figures 1b-f). The overall structure is comprised of 14 Cu atoms protected by 3 $^{i}PrS^{-}$ ligands, 8 PPh_3 ligands, and 10 hydrides, stabilized by one BF_4^- anion (Figure 1b). The core configuration, shown in Figure 1c, is constructed from a combination of two interlocking tetrahedral geometries, with one tetrahedron nested within the other but oriented in the opposite direction. The arrangement involves 10 Cu atoms forming one tetrahedron and 4 Cu atoms forming the other (Figure 1d; henceforth referred to as Tetrahedra 1 and 2). The three thiolate ligands bridge the two tetrahedral geometries (Figure 1e). The core structure creates 8 positions at the vertices of the tetrahedra that accommodate 8 bulky PPh_3 ligands (Figures 1f & S5).

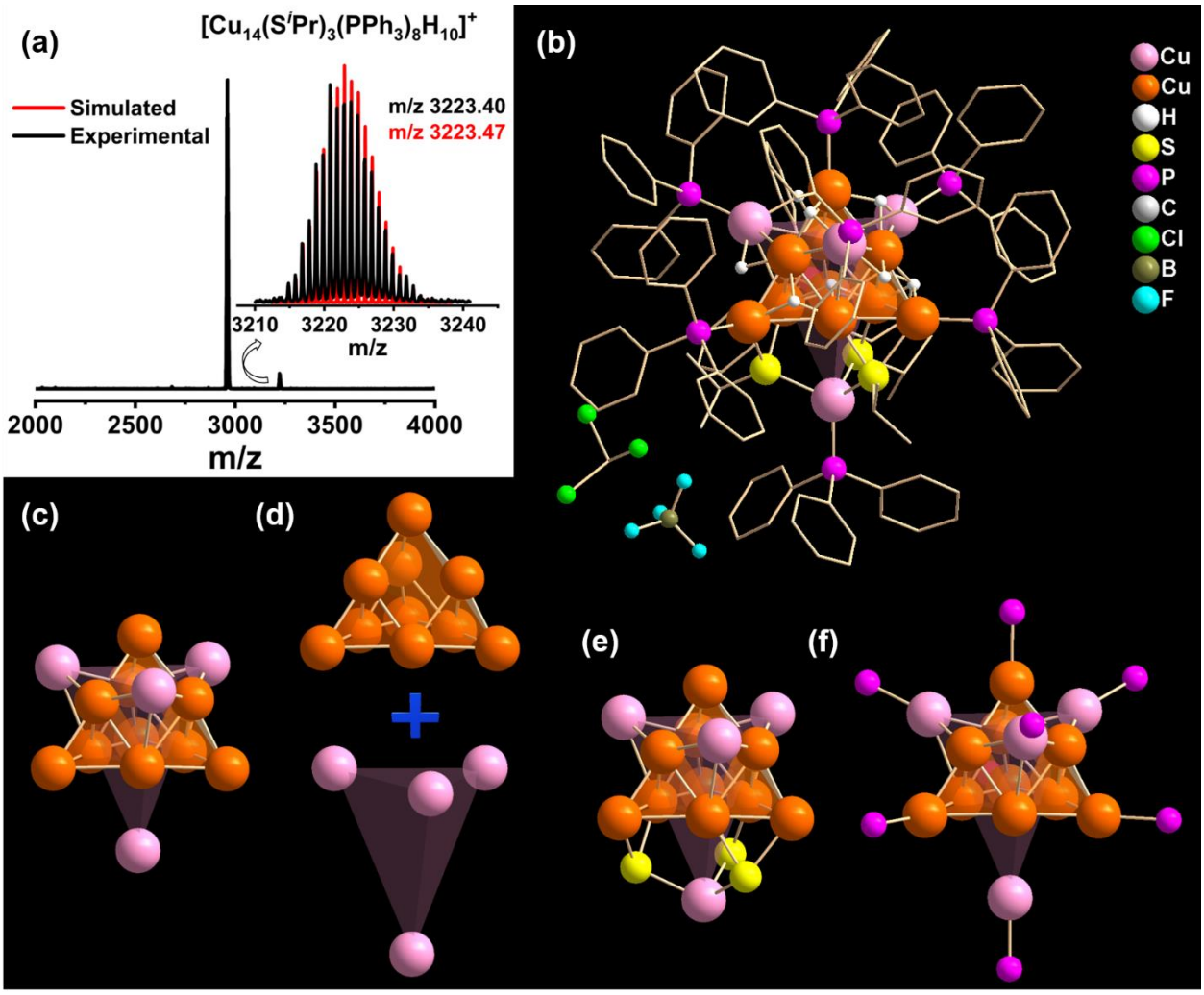

Figure 1. Common Underlying Geometric Structure. (a) Mass spectrum of $[Cu_{14}(^{i}PrS)_3(PPh_3)_8H_{10}]^+$. Inset: The measured (black trace) and simulated (red trace) isotopic patterns of $[Cu_{14}(^{i}PrS)_3(PPh_3)_8H_{10}]^+$.(b) Overall atomic structure of $[Cu_{14}(^{i}PrS)_3(PPh_3)_8H_{10}].BF_4.(CHCl_3)$ nanocluster (one of the conformers; Conformer C); H atoms of the protecting ligands are omitted for clarity. (c) Core comprising 14 Cu atoms. (d) The core structure is a fusion of two tetrahedral geometries: Tetrahedron 1 containing 10 Cu atoms and Tetrahedron 2 containing 4 Cu atoms. (e) Arrangement of S atoms connecting Tetrahedrons 1 and 2 in a μ_3 bridging fashion. (f) Each P atom is attached to the eight vertices of the interlocked two tetrahedral geometries of the Cu core. (b-f) Representative geometric architecture and atomic arrangement of all three conformers.

The detailed X-ray crystallographic data indicate the precise bond lengths and angles of each conformer. As an aid for visualization, in Figure 2a we have color-coded a set of distances within Tetrahedron 1 of the

representative structure. Notably, the lengths of all three highlighted blue Cu···Cu distances are identical within the conformer but differ when compared across three conformers. Likewise, the solid green, dotted red, and dotted purple distances exhibit the same pattern. These variations are quantitatively illustrated in Figure 2b. There are similar sets in remaining unhighlighted bonds which display variation in length but to a lesser extent (Figure S6). Six prominently varying bond angles are depicted in Figure 2c with corresponding Cu atom numbers shown in Figure 2a. A difference of up to 8 degrees is observed for some of the bond angles across the three conformers (Figure S7).

The arrangement of color-coded bonds is due to the underlying 120° symmetry of the core, a hallmark of tetrahedral geometry. Though the varying bond lengths and angles distort the tetrahedron, the core C_3 symmetry remains intact. This is further reflected in bond angles, such as <765 = <5(10)9 = <987 and <654 = <(10)93 = <872, among others. All bond lengths, angles, and their symmetry analogs for Tetrahedron 1 are presented in full detail in Supplementary Figures S6 & S7.

Additional structural differences avail themselves upon examining Tetrahedra 1 and 2 together (Figures 2d-f, S8). Distortions in the Cu skeleton are accompanied by changes in the Cu-S bond lengths and angles (Figures 2g-2h & S9-S10), as well as in the Cu-P bond lengths (Figure S11). The overlay of the two clusters in Figure 2i underscores the structural differences.

The distinction between conformers and structural isomers is well-established in small molecule chemistry.[1] The novelty in this example lies in its extension to the nanoscale, where such distinctions have been far less explored due to the inherent complexity and lack of atomic-level precision in most nanomaterials. Isomerism is of fundamental importance to structure-property relationships. Conformational isomerism constitutes perhaps the most subtle structural rearrangement that might reasonably result in a corresponding change in property. Two important previous studies demonstrated the ability to induce conformational changes *via* external stimuli such as applied pressure, allowing researchers to observe how these changes directly impact physical properties.[29,30] These methods are powerful because they start with a single, well-defined conformer, enabling precise structure-property correlations in "phase-pure" systems. In contrast, our approach offers a complementary perspective: instead of requiring external stimuli, the system naturally stabilizes multiple conformers within the same crystal lattice. While this might limit the ability to study each conformer in isolation, it provides a rare opportunity to examine how such structural diversity emerges spontaneously, and to study the collective properties of a system with intrinsic conformational heterogeneity. Furthermore, the coexistence of conformers could inspire future methods for selectively isolating or stabilizing individual conformations under controlled conditions.

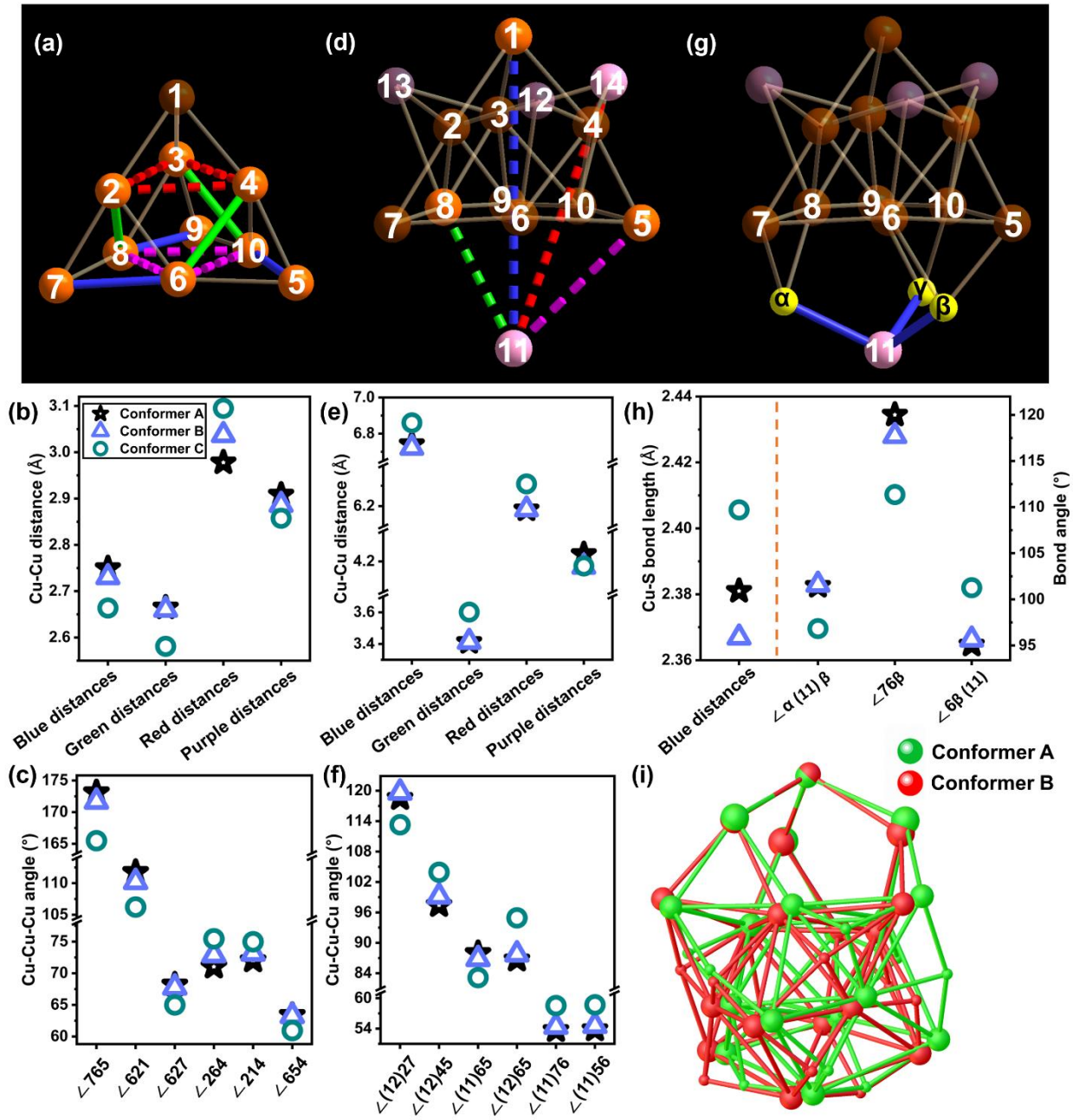

Figure 2. Conformational Isomerism. The variation in bond lengths and angles results in three conformers (conformer A, B, and C). (a) Illustration of four sets of bonds exhibiting significant variations in Tetrahedron 1. Cu atoms are numbered for angle representation. (b) Corresponding bond lengths that underscore the differences between these conformers. (c) Six selected bond angles showing substantial differences across the conformers. Together, Figures (a-c) provide a visualization of the structural differences within Tetrahedron 1 among the conformers. Likewise, Figures (d-f) present Cu-Cu distances and angles in Tetrahedron 1 and 2 combined. (g,h) Along with the Cu skeleton, Cu-S bond lengths and angles vary among the three conformers. (i) The overlay of $Cu_{14}S_3H_{10}$ moiety of clusters A and B captures

structural changes. Cluster C is omitted for better representation. The Cu-Cu distances greater than 2.88 Å are denoted in dotted lines. Color label: deep/transparent orange-Cu in Tetrahedron 1; deep/transparent rose-Cu in Tetrahedron 2; and yellow-sulfur.

In addition, each conformer exhibits chirality. We illustrate the origin of chirality using cluster C as a representative example (Figure 3). A perfect tetrahedral geometry exhibits mirror symmetry and is thus achiral. However, in our case, non-vertex copper atoms shift towards one side, breaking this mirror symmetry (Figures 3a-d & S13, S14). For easier visualization we resort to two-dimensional representation. We focus on one side plane (Figure 3a) and the bottom plane (Figure 3c) of Tetrahedron 1 to highlight the structural deviation from the tetrahedral symmetry. The loss of mirror symmetry transforms the copper core into a chiral entity (Figure S15).

Apart from the core distortion, the arrangement of thiol ligands also contributes to the chirality of the clusters (Figures 3e, S16). The three S atoms are arranged in an equilateral triangular fashion. The askew orientation of this triangle relative to the bottom plane of the Tetrahedron 1 establishes another source of chirality. While both core distortion and thiol arrangement disrupt the mirror symmetry, the 120° rotational symmetry persists (Figure 3f). It is interesting to note that the chiral mirror-images can be interchanged without breaking and reattaching bonds. In the context of small organic molecules, conformers with non-superposable mirror images (*e.g.,* 6,6'-dinitro-2,2'-diphenic acid) are called atropisomers.[22,31,32] Here we extend the concept of atropisomerism to our nanoscale structure.

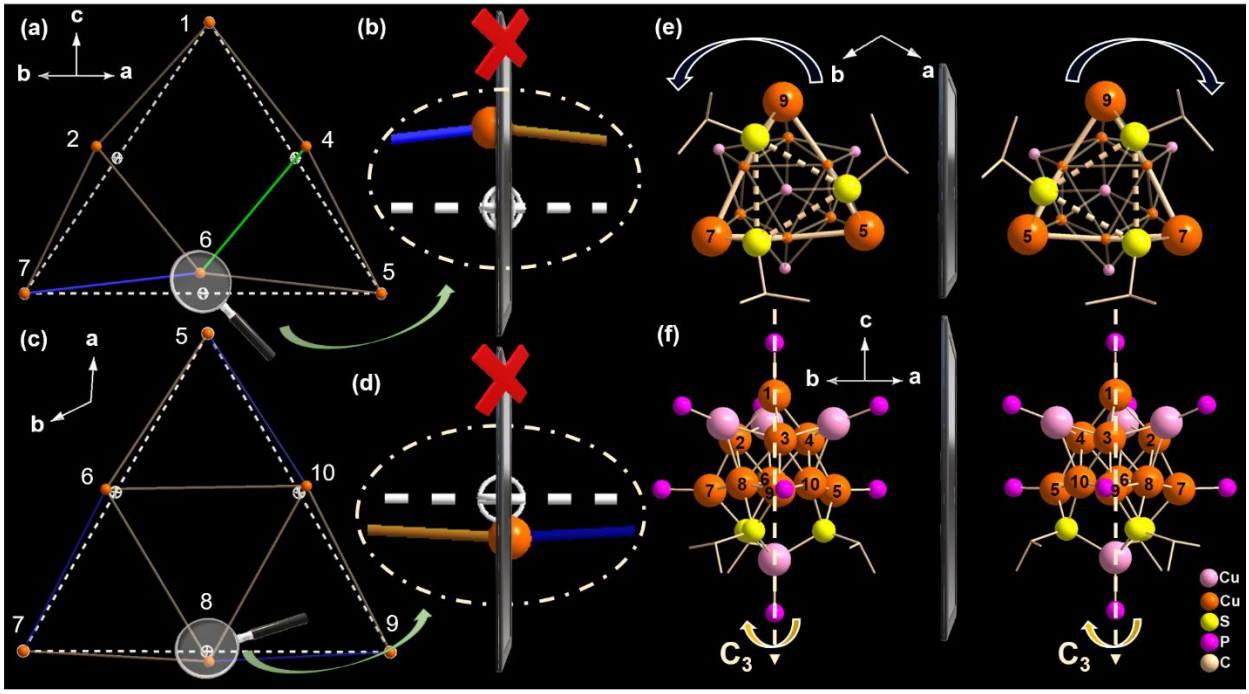

Figure 3. Stereo Isomerism. All three conformers are chiral. One of the conformers (cluster C) is chosen to illustrate the emergence of chirality. Chirality originates from the distortion of tetrahedron 1 and the arrangement of thiolate ligands. (a-d) The structural distortion of Tetrahedron 1 (solid lines, solid orange spheres) relative to the standard tetrahedral geometry (dashed white lines, hollow white spheres) breaks the symmetry and hence its mirror images are non-super-imposable. (a, b) Side face of tetrahedron 1. (c, d) Bottom layer of tetrahedron 1. Blue and Green bonds are the same ones as in Figure 2a. Numbering of atoms taken from Figure 2a for consistency. (e) Relative orientation of the equilateral triangle made by three S atoms with respect to the bottom plane of the Tetrahedron 1 makes mirror images non-super-imposable. Thick solid and dotted lines are for easy visualization. (f) Side view of the Cu_{14} NC. Phenyl rings and hydrides are omitted for clear visualization.

The fact that the three chiral conformers solidify into the same co-crystal is worthy of further discussion. Among the 500-plus known metal NCs, only a select few have been observed to co-crystallize.[33] One notable previous study exploits co-crystallization to realize physical and chemical properties distinct from those of the individual constituents.[34] Co-crystallization has facilitated structural characterization of the conformers of a small molecule.[35] Another notable study utilized a co-crystallization agent to obtain conformers of caffeine through engineering of the crystal energy landscape.[36] The co-crystallization of isomeric nanoclusters bearing different energies has been predicted from theory,[37] but to our knowledge has not been observed experimentally until now.

Figure 4a provides a visual representation of how these three conformers come together, assembling in a hexagonal pattern within the trigonal crystal lattice, forming hierarchically ordered structures. A broader view in Figure 4b showcases the hexagonal unit comprised of all three conformers, with the repetition of this unit leading to the overall crystal packing along the c direction. In this arrangement, cluster B consistently aligns directly above another B, while clusters A and C alternate positions in an A-C-A-C sequence within the three-dimensional lattice. As a result, each unit cell contains all three conformers, as depicted in Figure 4c. Further examination of the packing structure along the a, b, and c directions, as detailed in Figure S17, reveals an *ABA* stacking pattern (italics here denote the usual notational convention for stacking layers, not to be confused with clusters A and B), resulting in a hexagonal close-packing arrangement within the crystal lattice. The crystal used in our X-ray diffraction analysis displayed a Flack parameter of 0.06, indicating that in 6% of cases, chiral enantiomers of opposite handedness replace the original ones.

Figure 4d highlights the non-covalent interactions that might contribute to this complex assembly. The interactions between clusters A and C and between B and C appear to be dominated by C-H···H-C interactions originating from the phenyl rings of the PPh_3 ligands. The interactions between clusters A and B appear to mostly be governed by C-H···π interactions. Figure 4e further illustrates the supramolecular interactions between the *A* and *B* layers in the crystal lattice.

The three conformational isomers and their mirror images together give us six snapshots of the underlying fluxionality. Fluxionality for small molecules is typically inferred from line broadening in liquid-state spectroscopy.[49,50] Here we manage to capture glimpses of the underlying fluxionality in a single solid-state structure.

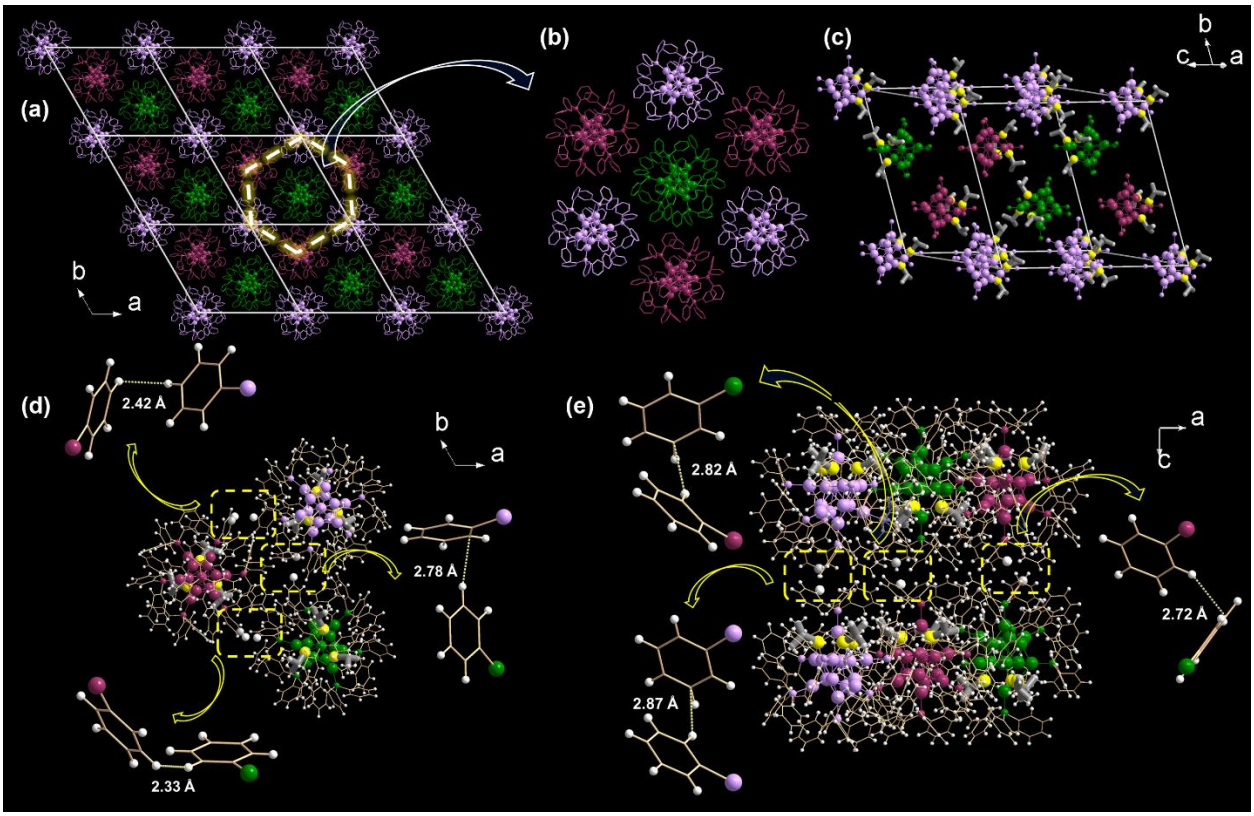

Figure 4. Co-crystallization of conformers and Inter-cluster non-covalent interactions. (a) Superlattice packing of all three conformers with a hexagonal arrangement in a 3 × 3 × 3 cell viewed along the c-axis. (b) Zoom-in images of the layer in Figure a. The packing is such that when viewed along the c-axis, all three conformers coexist in a layer. In the c-direction, clusters B are always stacked one on top of another. Whereas cluster A and cluster C are stacked in –A-C-A-C-A- pattern. (c) Ultimately, all three conformers co-crystallize within the same unit cell. (d) Non-covalent C-H…π and C-H…H-C interactions among the conformers in the ab plane and (e) in the ac plane. Color label: green-cluster A; lavender-cluster B; violet-cluster C; yellow-sulfur; and golden stick-carbon. The carbon tails of the thiolate ligands are highlighted for better visualization for Figures c-e.

Conclusion

In summary, we report the atomic structures of three chiral conformers of an atomically precise metal nanocluster. We believe this to be the first observation of atropisomerism in nanoclusters. The fact that all

three chiral conformers were observed to co-crystallize suggests a future direction for the theoretical investigation of packing energies. Also, in future work it will be interesting to correlate these structural variations with differences in physical and chemical properties known to intimately depend on nanocluster structure, like photoluminescence, circular dichroism, and catalytic activity.[29,30,38-48] In a sense, the differences among a set of conformational isomers represent something like the minimal units of structural change that might yield dissimilarity in such physio-chemical properties. In other words, this system could serve as a testbed for structure-property correlations of nanoclusters.[29,30,38,39] While we reserve the direct investigation of such properties for future work, the current study establishes a robust basis for such analyses.

Methods

Synthesis of $[Cu_{14}(^{i}PrS)_3(PPh_3)_8H_{10}][BF_4]$ NC

Initially, 50 mg (0.16 mmol) of $Cu(CH_3CN)_4BF_4$ and 50 mg (0.19 mmol) of PPh_3 were mixed in the mixture solution of 2 mL acetonitrile and 0.5 mL chloroform at room temperature and stirred until a clear solution was obtained. After that, 15 µL (0.16 mmol) of ^{i}PrSH was added to the mixture and continued stirring. After 15 min of stirring, 50 mg (1.32 mmol) of $NaBH_4$ dissolved in 2.5 mL methanol was added into the mixture, and a reddish orange color solution was formed. Then the reaction was kept for another 1 h under continuous stirring. After completion, the reaction mixture was centrifuged, and the orange precipitate was formed. After drying properly, the precipitate was dissolved in the solvent mixture of chloroform/hexane (volume ratio 1:1). The final clear solution was kept for crystallization at ambient conditions. After 5 days, yellow prism-shaped crystals were obtained.

Synthesis of $[Cu_{14}(^{i}PrS)_3(PPh_3)_8D_{10}]^{+}$ ($Cu_{14}D$) NC

The same procedure was adopted, whatever was mentioned for the synthesis of the Cu_{14} NC. Instead of $NaBH_4$, we have used $NaBD_4$ as a reducing agent.

Author contributions

A.K.D. performed the synthesis. A.K.D and S.H did the characterization, data analysis, data interpretation and wrote the manuscript. T.J.W performed single crystal diffraction measurements. V.S.W. contributed to

ESI-MS analysis. All authors discussed the results. M.P.B supervised the overall work. Authors declare no conflict of interest.

Acknowledgments

This work was supported by Beckman Young Investigator Award. Authors would like to thank Dr. Lingyang Zhu (Department of Chemistry, University of Illinois Urbana-Champaign) for NMR spectroscopy and further useful discussions, Dr. Danielle L. Gray (Department of Chemistry, University of Illinois Urbana-Champaign) for useful suggestions on crystallographic analysis, and Dr. Majed S. Fataftah (Assistant Professor, Department of Chemistry, University of Illinois Urbana-Champaign) for fruitful suggestions during manuscript preparation.

References

1. Eliel, E. L.; Wilen, S. H. Stereochemistry of Organic Compounds. John Wiley & Sons, **1994**.
2. Billinge, S. J. L.; Levin, I. The Problem with Determining Atomic Structure at the Nanoscale. *Science* **2007,** *316,* 561-565.
3. Jadzinsky, P. D.; Calero, G.; Ackerson, C. J.; Bushnell, D. A.; Kornberg, R. D. Structure of a Thiol Monolayer-Protected Gold Nanoparticle at 1.1 Å Resolution. *Science* **2007,** *318,* 430-433.
4. Jin, R.; Zeng, C.; Zhou, M.; Chen, Y. Atomically Precise Colloidal Metal Nanoclusters and Nanoparticles: Fundamentals and Opportunities. *Chem. Rev.* **2016,** *116,* 10346-10413.
5. Chakraborty, I.; Pradeep, T. Atomically Precise Clusters of Noble Metals: Emerging Link between Atoms and Nanoparticles. *Chem. Rev.* **2017,** *117,* 8208-8271.
6. Cook, A. W.; Hayton, T. W. Case Studies in Nanocluster Synthesis and Characterization: Challenges and Opportunities. *Acc. Chem. Res.* **2018,** *51,* 2456-2464.
7. Biswas, S.; Das, S.; Negishi, Y. Advances in Cu Nanocluster Catalyst Design: Recent Progress and Promising Applications. *Nanoscale Horiz.* **2023,** *8,* 1509-1522.
8. Biswas, S.; Das, A. K.; Mandal, S. Surface Engineering of Atomically Precise M (I) Nanoclusters: From Structural Control to Room Temperature Photoluminescence Enhancement. *Acc. Chem. Res.* **2023,** *56,* 1838-1849.
9. Qian, H.; Zhu, M.; Wu, Z.; Jin, R. Quantum Sized Gold Nanoclusters with Atomic Precision. *Acc. Chem. Res.* **2012,** *45,* 1470-1479.
10. Zeng, C.; Chen, Y.; Kirschbaum, K.; Lambright, K. Jin, R. Emergence of Hierarchical Structural Complexities in Nanoparticles and their Assembly. *Science* **2016,** *354,* 1580-1584.
11. Matus, M. F.; Häkkinen, H. Understanding Ligand-Protected Noble Metal Nanoclusters at Work. *Nat. Rev. Mater.* **2023,** *8,* 372-389.

12. Zeng, C.; Chen, Y.; Liu, C.; Nobusada, K.; Rosi, N. L.; Jin, R. Gold Tetrahedra Coil up: Kekulé-like and Double Helical Superstructures. *Sci. Adv.* **2015,** *1,* e1500425.
13. Xia, N.; Yuan, J.; Liao, L.; Zhang, W.; Li, J.; Deng, H.; Yang, J.; Wu, Z. Structural Oscillation Revealed in Gold Nanoparticles. *J. Am. Chem. Soc.* **2020,** *142,* 12140-12145.
14. Tian, S.; Li, Y-Z.; Li, M-B.; Yuan, J.; Yang, J.; Wu, Z.; Jin, R. Structural Isomerism in Gold Nanoparticles Revealed by X-ray Crystallography. *Nat. Commun.* **2015,** *6,* 8667.
15. Kang, X.; Zhu, M. Structural Isomerism in Atomically Precise Nanoclusters. *Chem. Mater.* **2020,** *33,* 39-62.
16. Guan, Z-J.; Hu, F.; Li, J-J.; Wen, Z-R.; Lin, Y-M.; Wang, Q-M. Isomerization in Alkynyl-Protected Gold Nanoclusters. *J. Am. Chem. Soc.* **2020,** *142,* 2995-3001.
17. Chen, Y.; Liu, C.; Tang, Q.; Zeng, C.; Higaki, T.; Das, A.; Jiang, D-E.; Rosi, N. L.; Jin, R. Isomerism in $Au_{28}(SR)_{20}$ Nanocluster and Stable Structures. *J. Am. Chem. Soc.* **2016,** *138,* 1482-1485.
18. Zhuang, S.; Liao, L.; Yuan, J.; Xia, N.; Zhao, Y.; Wang, C.; Gan, Z.; Yan, N.; He, L.; Li, J.; Deng, H.; Guan, Z.; Yang, J.; Wu, Z. Fcc versus Non-fcc Structural Isomerism of Gold Nanoparticles with Kernel Atom Packing Dependent Photoluminescence. *Angew. Chem. Int. Ed.* **2019,** *58,* 4510-4514.
19. Zhang, C.; Wang, Z.; Si, W-D.; Wang, L.; Dou, J-M.; Gao, Z-Y.; Tung, C-H.; Sun, D. Solvent-Induced Isomeric Cu_{13} Nanoclusters: Chlorine to Copper Charge Transfer Boosting Molecular Oxygen Activation in Sulfide Selective Oxidation. *ACS Nano* **2022,** *16,* 9598-9607.
20. Li, Y.; Higaki, T.; Du, X.; Jin, R. Chirality and Surface Bonding Correlation in Atomically Precise Metal Nanoclusters. *Adv. Mater.* **2020,** *32,* 1905488.
21. Crippen, G. M.: Havel, T. F. Distance Geometry and Molecular Conformation. Vol. 74. Taunton: Research Studies Press, 1988.
22. Loudon, M. ORGANIC CHEMISTRY 6E., **1988**.
23. Kalsi, P. S. Stereochemistry Conformation and Mechanism. New Age International, **2005**.
24. Hoffmann, R. W. Flexible Molecules with Defined Shape—Conformational Design. *Angew. Chem. Int. Ed.* **1992,** *31,* 1124-1134.
25. Doshi, U.; McGowan, L. C.; Ladani, S. T.; Hamelberg, D. Resolving the complex role of enzyme conformational dynamics in catalytic function. *Proc. Natl. Acad. Sci.* **2012,** *109,* 5699-5704.
26. Gan, Z.; Liu, Y.; Wang, L.; Jiang, S.; Xia, N.; Yan, Z.; Wu, X.; Zhang, J.; Gu, W.; He, L.; Dong, J.; Ma, X.; Kim, J.; Wu, Z.; Xu, Y.; Li, Y.; Wu, Z. Distance Makes a Difference in Crystalline Photoluminescence. *Nat Commun.* **2020,** *11,* 5572.
27. Wang, M.; Xia, S.; Jiang, C.; He, S.; Xia, J.; Wang, Z.; Yuan, X.; Liu, L.; Chen, J. Aggregation Inducing Reversible Conformational Isomerization of Surface Staple in $Au_{18}SR_{14}$ Nanoclusters. *Small* **2024,** *20,* 2311895.
28. Zeng, S.; Ge, X.; Deng, H.; Hao, S.; Zhang, Z.; Teo, B. K.; Sun, C. Synthesis and Structure of Polyhydrido Copper Nanocluster $[Cu_{14}H_{10}(PPh_3)_8(SPhMe_2)_3]^+$: Symmetry-Breaking by Thiolate Ligands to form Racemic Pairs of Chiral Clusters in Solid-State. *J. Clust Sci.* **2024,** *35,* 109-113.
29. Li, Q.; Mosquera, M. A.; Jones, L. O.; Parakh, A.; Chai, J.; Jin, R.; Schatz, G. C.; Gu, X. W. Pressure-Induced Optical Transitions in Metal Nanoclusters. *ACS Nano* **2020,** *14,* 11888-11896.
30. Li, Q.; Zeman, C. J. I. V.; Kalkan, B.; Kirschbaum, K.; Gianopoulos, C. G.; Parakh, A.; Doan, D.; Lee, A. C.; Kulikowski, J.; Schatz, G. C. Direct Observation of the Pressure-Induced Structural Variation in Gold Nanoclusters and the Correlated Optical Response. *Nano Lett.* **2023**, *23*, 132– 139.

31. Christie, G. H.; Kenner, J. LXXI.—The Molecular Configurations of Polynuclear Aromatic Compounds. Part I. The Resolution of γ-6: 6′-Dinitro-and 4: 6: 4′: 6′-Tetranitro-Diphenic Acids into Optically Active Components. *J. Chem. Soc., Trans.* **1922,** *121,* 614-620.
32. Kuhn, R. Molekulare Asymmetrie. Stereochemie 803, **1933**.
33. Kang, X.; Zhu, M. Cocrystallization of Atomically Precise Nanoclusters. *ACS Mater. Lett.* **2020,** *2,* 1303-1314.
34. Bodiuzzaman, M.; Dar, W. A.; Pradeep, T. Cocrystals of Atomically Precise Noble Metal Nanoclusters. *Small* **2021,** *17,* 2003981.
35. Song, C. E.; Kim, Y. H.; Kim, K. M.; Chi, D. Y.; Jeong, J. H. Cocrystallization of Two Conformers of (2S, 3S, 9S, 10S)-2, 3, 9, 10-tetraphenyl-1, 4, 8, 11-tetraoxacyclotetradecane-6, 13-dione. *Acta Crystallogr. C* **1999,** *55,* 1574-1575.
36. Habgood, M.; Price, S. L. Isomers, Conformers, and Cocrystal Stoichiometry: Insights from the Crystal Energy Landscapes of Caffeine with the Hydroxybenzoic Acids. *Cryst. Growth Des.* **2010,** *10,* 3263–3272.
37. Schaefer, B.; Pal, R.; Khetrapal, N. S.; Amsler, M.; Sadeghi, A.; Blum, V.; Zeng, X. C.; Goedecker, S.; Wang, L-S. Isomerism and Structural Fluxionality in the Au_{26} and Au_{26}^- Nanoclusters. *ACS Nano* **2014,** *8,* 7413-7422.
38. Aikens, C. M. Electronic and Geometric Structure, Optical Properties, and Excited State Behavior in Atomically Precise Thiolate-Stabilized Noble Metal Nanoclusters. *Acc. Chem. Res.* **2018,** *51,* 3065-3073.
39. Biswas, S.; Das, A. K.; Reber, A. C.; Biswas, S.; Bhandary, S.; Kamble, V. B.; Khanna, S. N.; Mandal, S. The New Ag–S Cluster $[Ag_{50}S_{13}(S^tBu)_{20}][CF_3COO]_4$ with a Unique hcp Ag_{14} Kernel and Ag_{36} Keplerian-Shell-Based Structural Architecture and Its Photoresponsivity. *Nano Lett.* **2022,** *22,* 3721-3727.
40. Shi, W-Q.; Zeng, L.; He, R-L.; Han, X-S.; Guan, Z-J.; Zhou, M.; Wang, Q-M. Near-Unity NIR Phosphorescent Quantum Yield from a Room-Temperature Solvated Metal Nanocluster. *Science* **2024,** *383,* 326-330.
41. Kang, X.; Zhu, M. Tailoring the Photoluminescence of Atomically Precise Nanoclusters. *Chem. Soc. Rev.* **2019,** *48,* 2422-2457.
42. Chen, T.; Yang, S.; Chai, J.; Song, Y.; Fan, J.; Rao, B.; Sheng, H.; Yu, H.; Zhu, M. Crystallization-Induced Emission Enhancement: A Novel Fluorescent Au-Ag Bimetallic Nanocluster with Precise Atomic Structure. *Sci. Adv.* **2017,** *3,* e1700956.
43. Lu, J.; Shao, B.; Huang, R-W.; Arzaluz, L. G.; Chen, S.; Han, Z.; Yin, J.; Zhu, H.; Dayneko, S.; Hedhili, M. N.; Song, X.; Yuan, P.; Dong, C.; Zhou, R.; Saidaminov, M. I.; Zang, S-Q.; Mohammed, O. F.; Bakr, O. M. High-Efficiency Circularly Polarized Light-Emitting Diodes Based on Chiral Metal Nanoclusters. *J. Am. Chem. Soc.* **2024,** *146,* 4144-4152.
44. Liang, X-Q.; Li, Y-Z.; Wang, Z.; Zhang, S-S.; Liu, Y-C.; Cao, Z-Z.; Feng, L.; Gao, Z-Y.; Xue, Q-W.; Tung, C-H.; Sun, D. Revealing the Chirality Origin and Homochirality Crystallization of Ag_{14} Nanocluster at the Molecular Level. *Nat. Commun.* **2021,** *12,* 4966.
45. Tsunoyama, H.; Sakurai, H.; Negishi, Y.; Tsukuda, T. Size-Specific Catalytic Activity of Polymer-Stabilized Gold Nanoclusters for Aerobic Alcohol Oxidation in Water. *J. Am. Chem. Soc.* **2005,** *127,* 9374-9375.
46. Sun, C.; Mammen, N.; Kaappa, S.; Yuan, P.; Deng, G.; Zhao, C.; Yan, J.; Malola, S.; Honkala, K.; Häkkinen, H.; Teo, B. K.; Zheng, N. Atomically Precise, Thiolated Copper–Hydride Nanoclusters

as Single-Site Hydrogenation Catalysts for Ketones in Mild Conditions. *ACS Nano* **2019,** *13,* 5975-5986.
47. Higaki, T.; Li, Q.; Zhou, M.; Zhao, S.; Li, Y.; Li, S.; Jin, R. Toward the Tailoring Chemistry of Metal Nanoclusters for Enhancing Functionalities. *Acc. Chem. Res.* **2018,** *51,* 2764-2773.
48. Biswas, S.; Negishi, Y. A Comprehensive Analysis of Luminescent Crystallized Cu Nanoclusters. *J. Phys. Chem. Lett.* **2024,** *15,* 947-958.
49. Drago, R. S. Physical Methods in Chemistry (2nd ed.). Philadelphia: W. B. Saunders, **1977**.
50. Gill, G.; Pawar, D. M.; Noe, E. A. Conformational Study of cis-1, 4-di-tert-butylcyclohexane by Dynamic NMR Spectroscopy and Computational Methods. Observation of Chair and Twist-Boat Conformations. *J. Org. Chem.* **2005,** *70,* 10726-10731.

TOC